IEEE Open Journal of
Power Electronics

Received 11 July 2023; revised 1 September 2023; accepted 18 September 2023. Date of publication 25 September 2023;
date of current version 4 October 2023. The review of this paper was arranged by Associate Editor Lingxiao Xue.

Digital Object Identifier 10.1109/OJPEL.2023.3318896

Robust Optimization of a Wireless Power Transfer Coupler Against Manufacturing and Fabrication Tolerances

SAMPATH JAYALATH (Member, IEEE), AND AZEEM KHAN (Senior Member, IEEE)

Department of Electrical Engineering, University of Cape Town, Cape Town 7700, South Africa

CORRESPONDING AUTHOR: SAMPATH JAYALATH (e-mail: sampath.jayalath@uct.ac.za)

This work was supported in part by the National Research Foundation of South Africa, in part by the University of Cape Town, and in part by the Department of Science and Innovation of South Africa.

ABSTRACT The design variables are optimized to improve the overall performance of wireless power transfer (WPT) coils or couplers. However, failure to consider their uncertainties and tolerances will lead to variations in the performance targets of a WPT system and mass-scale production of couplers cannot afford performance variation from one coupler to another. Therefore, this article proposes a stochastic-based optimization method to incorporate the uncertainties and tolerances of design variables into the optimization process to realize a robust WPT coupler. The proposed robust optimization methodology is compared with the existing deterministic optimization methodology to achieve reduced transmitter and receiver side current harmonics, maximum efficiency, and minimum leakage magnetic field. The results demonstrate that the design resulting from the robust optimization has 1.59% and 1.66% fewer harmonics distortion in the receiver and transmitter side currents compared to the deterministic optimization, along with coil-to-coil efficiency of 96.5% and leakage field of 7.4 μT measured 650 mm from the center of the coupler. Moreover, the fabricated coupler from robust optimization has a superior efficiency profile under load variations.

INDEX TERMS Coil design, electric vehicles, inductive power transfer, multi-objective optimization, robust optimization, sensitivity analysis, wireless power transfer, tolerances.

I. INTRODUCTION

Inductive power transfer (IPT) technology is key to fully autonomous electric vehicles (EV), where conventional conductive chargers are replaced with IPT chargers. The coupler or the coils is the heart of an IPT charger. Coils with different geometrical shapes and winding arrangements are proposed to improve the objectives such as coupling coefficient, mutual inductance, quality factor, power density, and efficiency while reducing the cost, weight, and leakage magnetic field [1]. Moreover, the coil design must consider constraints such as the coil's area, air gap, frequency of operation, coupler material properties, and converter ratings [1]. Most limits on coil design objectives and constraints are defined in the SAE J2954 EV standard [2]. WPT system optimization problems usually take two approaches. One approach is to optimize the coupler or coil design variables, while the other is to optimize the WPT system parameters, such as coil inductances and compensation capacitors. However, this article focuses on the optimization of the design variables of the coupler.

Multi-objective optimization techniques are introduced to solve these coil optimization problems with multiple objectives and constraints, as shown in Table 1. Table 1 also summarizes the power ratings, finite element analysis (FEA) models, and optimization algorithms used for circular couplers. They search for the best design variables that meet the objectives and comply with the constraints of the design. Both analytical and numerical methods are proposed to optimize the IPT couplers [3], [4], [5], [6], [7], [8], [9], [10], [11], [12], [13].

The IPT coupler optimization proposed in the literature is carried out for deterministic model properties, as shown in Table 1, where uncertainties and tolerances of the design variables are ignored [3], [4], [5], [6], [7], [8], [9], [10], [11], [12], [13]. Therefore, solutions are not robust. Circular coils

TABLE 1. Proposed Multi-Objective Optimization Solutions For Circular Coil Structures

Ref	Power	DV	Constraints	Objectives	FEA	Algorithm	Uncertainties	Sens	Robust	Variation	
[3]	5 kW	D_c, A_{cu}, f, d_i	T	η, α, B_s	2D	PO using FEA and analytical	*No*	*No*	*No*	L_{Tx}:+6.5%	B_s :11.5%
										L_{Rx}:+3%	η:-0.48%
										k:+6.1%	
[4]	1-2 kW	N, r_i, h_{wf}	I_s, r_o, P	k and Q	2 D	NSGA II & PO	*No*	*No*	*No*	*NA*	
[5]	100 W	N_T, r_i, r_c	*NA*	η, B_s	NA	Lump loop model & PF	*No*	*No*	*No*	L_{Tx}:-4.1%	B_s:12.5%
										L_{Rx}:-2.4%	η:0%
										k :+4.6%	
[6]	3 kW	N, r_i, r_c	P_o, f,G, h	η, P_o, h	NA	NSGA II & PO	*No*	*No*	*No*	*NA*	
[7]	1 kW	f, l_f, r_f, $(2r_i)$ W_c^*	G, B_s ,Q_{CL}	η, C_T, D_h^*	2D	NSGA II & PO	*No*	*No*	*No*	L_{Tx}:10.4%	η:5.8%
										L_{Rx}:10.4%	C_T :NA
										k:NA	D_h:NA
[9]	1 kW	N, r_i , r_0, t_w	k, G, Q_{CL}	η_{coil}, B_s	2D	Analytical	*No*	*No*	*No*	L_{Tx}:+13%	η_{coil}:-2.4%
										L_{Rx}:+7%	B_s:±10%
										k:-3%	

Note: Most of the design variables are defined according to the nomenclature used in **Fig. 4**. NSGA II = Nondominated Sorting Genetic Algorithm II, , *PF*=Pareto Front, *PO*= Pareto Optimization, *G*- Geometrical constraints, r_w^* considered as a square shape conductor, N_T- Turn distribution, W_c- width of the coil, C_T-cost of the coil, D_h^*-Horizontal misalignment tolerance. Q_{CL}-Converter limitations, t_w-thickness of coil winding. DV: Design variables, FEA- Finite Element Analysis, Sens – Sensitivity analysis, Robust -Robustness and Ref-references.

are compared in Table 1 as it is the frequently used coupler, and observations are valid for other coupler structures such as DD, DDQ, BBP, and tripolar [8], [11], [12]. The design variable uncertainties arise from the coils' manufacturing and fabrication tolerances (MFT). The conductor's diameter, ferrite's dimensions, and passive shield's dimensions vary by a few millimeters from the designed optimized values due to inaccuracies in these components' manufacturing process. The space between two conductors in a winding, starting radius of a coil, ferrite placement, etc., also varies from their optimized values during the coil fabrication process. These variations contribute to the MFT of the coils. These tolerances are found in every industrial manufacturing process.

The failure to consider uncertainties of design variables during the optimization process will push the optimized design into extreme boundaries of the optimization space and has the risk of violating design objectives and constraints when implemented, as the exact values of the optimized design variables may not be precisely realizable during the production process due to abovementioned uncertainties and tolerances. In a series-series compensated IPT system, the coupling coefficient is restricted during optimization to be less than the critical coupling coefficient to avoid bifurcation [3], [9]. However, there is always the risk of violating such constraints for designs closer to the boundary of critical coupling. An increase in total harmonic distortion in the implemented WPT system is reported in [9] due to violations of constraints in the implemented system compared to simulations. Moreover, efficiency deviations in the implemented design by a large margin are reported in [7] compared to the optimized/simulated design. Such variations question the validity of solutions resulting from conventional deterministic multi-objective optimization (DMOO). These deviations are also evident from Table 1, as the fabricated coupler's objectives and parameters vary significantly (maximum of 13%) compared to the simulation results from the optimization process [3], [4], [5], [6], [7], [8], [9]. Deviations in objectives and constraints may result in poorly performing IPT chargers [3], [7], [9].

The cause of these variations is unlikely to occur due to the tolerances of measurement instruments such as LCR meters and power analyzers, as they have a worst-case tolerance of ±0.5%. One might avoid these performance deviations by altering the design variables in a laboratory environment. However, such activities question the validity of the DMOO process and design methodology, and one cannot follow a trial-and-error approach in mass-scale production in a commercial environment. Mass-scale production of WPT couplers requires a formalized design approach that can quantify these uncertainties and tolerances at the design stage to ensure that the fabricated coupler is operating as intended during the design stage.

Therefore, this article proposes a method to include the design variable uncertainties in the optimization process to realize a robust multi-objective optimization (RMOO) process. The optimization problem is formulated to achieve a WPT system with high efficiency, a lower leakage field, and lower total harmonics distortions (THD) in currents. Reducing the THD of an IPT system is beneficial as it impacts electromagnetic interference (EMI) issues. The designer must ensure all constraints related to THD are met to achieve lower THD. The proposed optimization method will ensure that all design objectives and constraints are met by the manufactured IPT system, even with the tolerances and uncertainties of design variables, to guarantee performance targets set during the design stage. Moreover, the effectiveness of the proposed methodology is compared with conventional DMOO.

The major contribution of this article compared to the existing literature is summarized as follows:

1) Introduces a method to quantify the impact of design variables on objectives and constraints using the design of experiment (DOE) technique.
2) Introduces a method to quantify tolerances of design variables of a WPT coupler. This is achieved by defining

each design variable's coefficient of variation by considering the manufacturing process's standard deviation determined via the process capability index.

3) Introduces safety margin to quantify failures or violations of design targets due to uncertainties and tolerances of design variables.
4) Introduces a method to incorporate reliability into the coil manufacturing process in terms of the number of defects per million designs in the short term.

II. IPT SYSTEM DESIGN

Initially, the impact of the power electronics system and compensation topology design requirements on the coil parameters, such as transmitter (L_{Tx}) and receiver side (L_{Rx}) inductances, mutual inductance (M), and coupling coefficient (k), is identified. These parameters usually depend on the operating frequency, rated load, voltage gain, etc., of the IPT system. This is critical as these requirements constrain coil parameters to achieve efficient operation of the IPT system. The proposed robust coil optimization was carried out once the impact of these requirements on the design parameters was identified. Because L_{Tx}, L_{Rx}, M, and k change with coils' design variables and their associated manufacturing and fabrication tolerances. In this article, the relationship is demonstrated for SS-compensation topology. However, similar relationships can be derived for other compensation topologies proposed in the literature [1].

A. IMPACT OF SS-COMPENSATION ON COUPLER DESIGN

The SS compensated IPT system shown in Fig. 1 is preferred for EV applications as the capacitances of Tx (C_{Tx}) and Rx coils (C_{Rx}) are independent of the coupling coefficient (k) and load variation, high efficiency at low k, etc. [14]. Fig. 1(a) shows the circuit model where S_1, S_2, S_3, and S_4 are semiconductor switches while D_1, D_2, D_3, and D_4 are fast recovery diodes. V_{DC} is the DC bus voltage supplied to the inverter. R_{Tx} and R_{Rx} are parasitic resistance of transmitter, and receiver coils with inductances L_{Tx} and $L_{Rx,}$ respectively. R_L is the equivalent load resistance of the battery.

Fig. 1(b) shows the simplified fundamental harmonic mutual inductive model of Fig. 1(a). M is the mutual inductance between the transmitter and receiver coils, and I_{Tx} and I_{Rx} are the currents in the transmitter and receiver side. The relationship between the input DC voltage (V_{DC}) and equivalent AC input voltage (V_s) or output voltage of the inverter can be defined as:

$$\hat{V}_s = \frac{4V_{dc}}{\pi} \sum_{n=1,3,5,..} \frac{\sin\left(nf_0 t_{on}\pi\right)}{n} \tag{1}$$

where n is the odd harmonic number and t_{on} is the ON time of the applied voltage pulse. Fundamental frequency (n=1) can be used to model the loosely coupled inductive power transfer system since the fundamental component is significantly larger than the harmonic components. The rectifier's output is usually connected across a battery bank, which can be approximated to a resistive load ($R_L = V_L^2/P$) with the power rating (P) equal to the rated power of the IPT system. V_L is the rated voltage across the load [3]. The ac equivalent resistance looking into the rectifier (R_{ac}) is given by:

$$R_{ac} = \frac{8}{\pi^2} R_L. \tag{2}$$

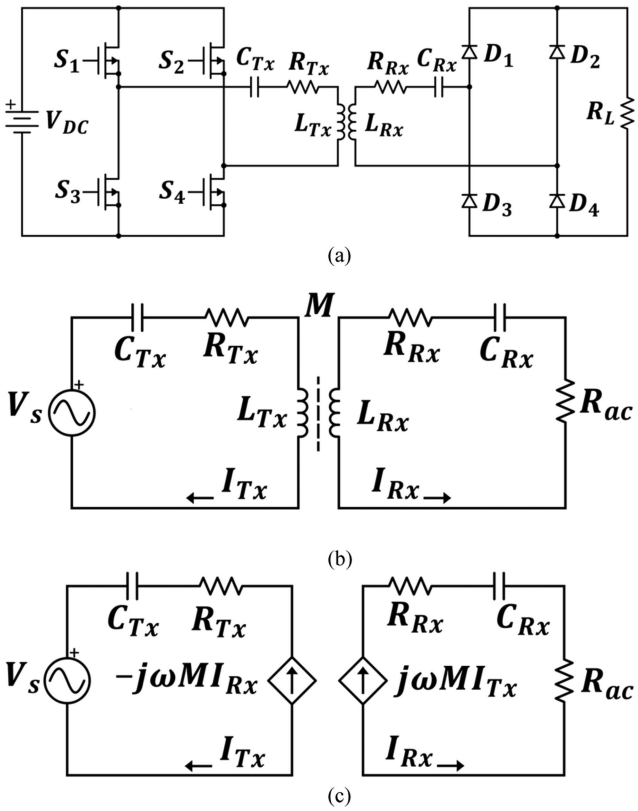

FIGURE 1. Series-series compensated IPT system: (a) Circuit model, (b) Simplified fundamental harmonic mutual inductive model, (c) Independent decoupled voltage source model.

Fig. 1(c) shows the independent decoupled voltage source model of the circuit shown in Fig. 1(a). The terms ($-j\omega MI_{\mathrm{Rx}}$) and ($-j\omega MI_{\mathrm{Tx}}$) are reflected impedances of the input and output side. The operating frequency (f_0) is given by:

$$f_0 = \frac{1}{2\pi \left(L_{Tx}C_{Tx}\right)^{1/2}} = \frac{1}{2\pi \left(L_{Rx}C_{Rx}\right)^{1/2}} \tag{3}$$

The coupling coefficient (k) of the coils is given by:

$$k = \frac{M}{\left(L_{Tx}L_{Rx}\right)^{1/2}} \tag{4}$$

The resonant inverter and rectifier of the IPT system have non-linear characteristics. As a result, it can cause harmonic distortion in the Tx-side and Rx-side currents. These distortions can interfere with the external electronic systems of the EV or radio signal receivers [9]. This article considers a class D rectifier, which is frequently used for IPT applications [1], [3], [8]. The harmonics of the I_{Rx} due to the nonlinearity of the class D rectifier can be minimized by satisfying the following

condition [15]:

$$\frac{\omega_0 L_{Rx}}{R_L} \approx \frac{8Q_e}{\pi^2} \geq 3 \tag{5}$$

where Q_e is the external quality factor $Q_e = (\omega_0 L_{Rx}/ R_{ac})$) Similarly, to reduce the harmonic distortion of the transmitter (Tx) current due to the non-linearity in the resonant inverter and the frequency bifurcation phenomena in the input impedance, the coupling coefficient for IPT systems that use D, E, and DE resonant converters should be limited to [9]:

$$k_0 \leq k_s \approx \frac{1}{\sqrt{2}Q_e} \ll k_c \approx \frac{1}{Q_e} \tag{6}$$

where k_0 is the coupling coefficient at the nominal position of the coils, k_c is the critical coupling coefficient, and k_s is the split coupling coefficient [9]. Equations (5) and (6) contain Q_e, which is a function of L_{Rx} [9]. Therefore, the range of L_{Rx} to meet the design criteria stipulated by (5) and (6) simultaneously can be found by:

$$\left(L_{Rx} \approx \frac{R_{ac}}{\sqrt{2}\omega_0 k_0}\right) \geq \left(\frac{3\pi^2 R_{ac}}{8\omega_0}\right) \tag{7}$$

The maximum value of k_0 that satisfies the equality given by (7) is given by [9]:

$$k_0 \leq k_{0m} = \frac{8}{3\pi^2}\sqrt{\frac{1}{2}} \tag{8}$$

Therefore, any design with a coupling coefficient higher than the k_{om} will increase harmonics, and the leakage magnetic field measured at a particular point from the coil [9]. Even though (8) restricts the k of the coil and its size, it is still important to maximize the coupling coefficient and quality factors of the coils to maximize the power transmission efficiency [3], [9]. The quality factor (Q_c) of a coil is given by:

$$Q_c \approx \frac{\omega L}{R_c} \tag{9}$$

L is the coil's inductance, while R_c is the parasitic AC resistance of the coil. Equation (9) assumes that the core and passive shielding losses are smaller than the copper losses [3]. The voltage transfer ratio ($V_{TR}(\omega_0)= V_{Rx1}/ V_{Tx1}$) between the input voltage (V_{Rx1}) and output voltage (V_{Tx1}) is critical for the safe operation of the IPT system, as it provides a guideline for the ratings of the semiconductor devices of the PE system [9]:

$$V_{TR}(\omega_0) \approx \sqrt{2}\sqrt{\frac{L_{Rx}}{L_{Tx}}} \tag{10}$$

The approximation in (10) considers $R_{Tx} << R_e$, $R_{Rx} << R_e$, and $k=k_0=k_s$ [9]. Since L_{Rx} is determined by (7), the size of the L_{Tx} depends on the selected $V_{TR}(\omega_0)$.

The requirement of low harmonic currents in the Tx and Rx side of the IPT systems can only be fulfilled if (5)–(8) are met by the coupler design, while (10) ensures the required voltage gain of the IPT system. Therefore, the coupler parameters such as k, L_{Tx}, and L_{Rx} are constrained by the inequalities (5)–(8) and (10). However, the uncertainties in design variables will impact the k, L_{Tx}, and L_{Rx}. Therefore, some of these constraints defined in (5)–(8) and (10) might be violated if the impact of uncertainties of design variables are ignored. These violations result in performance deviations compared to targeted performance levels. This impact is shown in Sections IV and V of this article by comparing the proposed robust and conventional deterministic optimization methods' designs.

B. LOAD DEPENDENCE CHARACTERISTICS

The load characteristics are derived at resonance. Therefore, the inductive and capacitive reactance at the primary and secondary are considered to cancel off each other. The reflected input impedance can be derived from Fig. 1(b) and (c) as:

$$Z_{ref} = -j\omega_0 M I_{Rx} = \frac{(\omega_0 M)^2}{Z_{Rx}} \tag{11}$$

Z_{Rx} is the secondary equivalent impedance given by $R_{Rx} + R_{ac}$. Moreover, the primary equivalent impedance (Z_{Tx}) will be equal to R_{Tx}. Using Kirchhoff's law, the transmitter current can be derived as:

$$I_{Tx} = \frac{V_s}{Z_{ref+}Z_{Tx}} = \frac{V_s\,(R_{Rx} + R_{ac})}{R_{Tx}\,(R_{Rx} + R_{ac}) + (\omega_0 M)^2} \tag{12}$$

$$I_{Rx} = \frac{j\omega_0 M I_{Tx}}{Z_{Rx}} = \frac{j\omega_0 M V_s}{R_{Tx}\,(R_{Rx} + R_{ac}) + (\omega_0 M)^2} \tag{13}$$

The output power of a SS-compensation system is given by:

$$P_o = |I_{Rx}|^2 R_{ac} \tag{14}$$

Therefore, it is evident that the output power increases with the increase in load. The efficiency (η_e) of the IPT system can be derived as:

$$\eta_e = \frac{P_{in}}{P_o} \tag{15}$$

where P_{in} is the input power given by ($V_s\, I_{Tx}$).

Equations (14) and (15) will be used to analyze the load independence characteristics of the designs resulting from the conventional DMOO and proposed RMOO.

III. OPTIMIZATION METHODOLOGY

Deterministic multi-objective optimization (DMOO) is preferred over single-objective optimization to improve the couplers' performance [3], [4], [5], [6], [7], [8], [9], [10], [11], [12], [13]. However, as discussed in Section I, the resulting designs may not be robust against the various coil's design variable tolerances. Therefore, this article proposes a robust multi-objective optimization (RMOO) method. This section outlines the theory in conventional DMOO and proposed RMOO methods.

A. DESIGN SPECIFICATIONS

Initially, the impact of the power electronics system and compensation topology design requirements on the coil parameters are identified. These requirements will vary for

different applications and compensation topologies. Section II derived the relationship for SS-compensation topology, and similar relationships can be derived for other compensation topologies proposed in the literature.

B. OPTIMIZATION PROBLEM FORMULATION

The next step of the proposed optimization process is identifying the design variables, design variables' tolerances, objectives, and constraints to formulate the optimization problem. They will vary depending on the designer's requirements. Design variables will depend on the coupler structures. The common coupler structures for EV are DD, DDQ, bipolar, tripolar, etc [1]. Most of the design variables are common to these couplers with minor variations. These common design variables are the separation between the turns, conductor radius, ferrite dimensions, separation between winding and ferrite, the separation between ferrite and passive shield, starting point of the windings, starting point of the ferrites, number of turns, and dimensions of the passive shield [1]. Moreover, these design variables have their associated fabrication and manufacturing tolerances except for the number of turns.

The common optimization objectives are efficiency, leakage magnetic field, area power density, volumetric power density, cost, weight, coils' quality factor, and coupling coefficient [1]. The designer can select which ones to optimize depending on their requirements. Constraints are usually determined based on the power electronics and compensation topology design requirements as demonstrated in Section II and industrial standards such as the SAE J2954 EV standard [2]. The design example shown in Section IV will explain how these objectives, design variables, and constraints are used to formulate the optimization problem.

C. SENSITIVITY ANALYSIS

The sensitivity analysis provides insight into the behavior of independent design variables on the performance of a given objective and constraint functions. If a particular design variable does not impact these functions, it can be excluded from the optimization process to simplify the problem and reduce the computational cost [17].

The next step is performing the optimization. This article provides steps of the conventional DMOO and proposed RMOO to demonstrate how manufacturing and fabrication tolerances or uncertainties can be incorporated into the design process.

D. DETERMINISTIC MULTI-OBJECTIVE OPTIMIZATION STEPS

The conventional DMOO will based on the following steps to determine the Pareto-front (PF) of the design [25].

- Minimize the functions:

$$f_n\left(d_1, d_2, \ldots . d_{k_d}\right) \rightarrow \min \tag{16}$$

- Provided that:

$$h_l\left(d_1, d_2, \ldots d_{k_d}\right) \leq 0;\ l = 1, 2, \ldots k_h \tag{17}$$

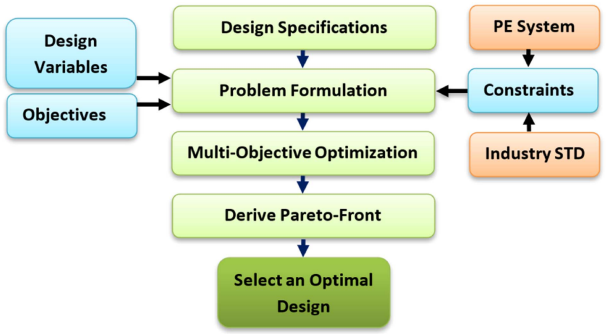

FIGURE 2. Deterministic multi-objective optimization (DMOO) flowchart for a wireless transfer coupler.

$$e_p\left(d_1, d_2, \ldots d_{k_d}\right) = 0;\ p = 1, 2, \ldots, k_e \tag{18}$$

- For design variables

$$d_j \in [d_L, d_U] \subset \mathbb{R}^{k_d} \tag{19}$$

$$d_L \leq d_j \leq d_U \tag{20}$$

where $f_n(d)$ is the optimization functions of the design with the constraint inequality functions $h_l(d_1, d_2, \ldots . d_{k_d})$ and the constraint equality function $e_p(d_1, d_2, \ldots . d_{k_d})$ for the vector of d_j=$(d_1, d_2, \ldots . d_{k_d})$ optimization variables. The PF of size y derived using each q iteration of the optimization algorithm is given by [16]:

$$P_q = \left\{f_{1ju}, \ldots \ldots, f_{aju}\right\} | u \in \mathbb{N}, 1 \leq \mathrm{u} \leq \mathrm{y} \tag{21}$$

Fig. 2 provides a summarized flowchart of a conventional DMOO proposed for wireless power transfer couplers [3], [4], [5], [6], [7], [8], [9], [10], [11], [12], [13]. The optimization problem is formulated by considering the design specification, design variables, objectives, and constraints. Then, the DMOO is performed using a suitable optimization algorithm to derive the PF. Finally, a Pareto-optimal design can be selected for implementation. It is important to note that sensitivity analysis was hardly considered in conventional DMOO and can be easily performed after the problem formulation.

E. ROBUST MULTI-OBJECTIVE OPTIMIZATION STEPS

The DMOO given by (16)–(20) does not incorporate stochastic restrictions (SR). Therefore, SRs are introduced in RMOO to ensure the predefined failure probabilities are not violated, and target variances are met. The design reliability can be expressed as [25], [26]:

$$1 - \frac{P\left(\mathcal{F}\right)}{P^T\left(\mathcal{F}\right)} \geq 0 \tag{22}$$

$P(\mathcal{F})$ is the probability of failure, while $P^{\mathrm{T}}(\mathcal{F})$ is the target probability. Equation (22) ensures that:

$$P\left(\mathcal{F}\right) = P\left[\{X : g_n\left(X\right) \leq 0\}\right] = \int_{\substack{k_r \\ \ldots . \\ g_n\left(x\right) \leq 0}} f_X\left(x\right) dx \tag{23}$$

will not exceed the predefined $P^{T}(\mathcal{F})$, under the consideration of random influences:

$$X = \left[X_1, X_1, \ldots., X_{k_r}\right]^T \tag{24}$$

where $f_X(x)$ is the joint probability density function of random variables and $n = 12,...,k_g$ limit state functions $g_n(x) \leq 0$. The following modifications (22)–(24) ensure that the design variables d_j in (19) satisfy the constraint given by (22) to predefined probabilities. Therefore, the design variables d_j becomes:

$$d = E\,[X] \tag{25}$$

are the means of the k_r random influences X. The objectives and constraints defined by (16)–(18) become non-deterministic functions due to random influences. Therefore, the objective (16) is improved with the requirement to minimize the variances $\sigma^2_{X_i}$ [26].

$$f_n\left(d_1, d_2, \ldots..d_{k_d}, \sigma^2_{X_1}, \sigma^2_{X_2}, \ldots, \sigma^2_{X_{k_r}}, P\left(\mathcal{F}\right)\right) \rightarrow \min \tag{26}$$

$$\text{Where,}\sigma^2_{X_i} = \frac{1}{M-1}\sum_{k=1}^{M}\left(x_i^k - \mu_{X_i}\right)^2 \tag{27}$$

It is important to evaluate the reliability of the final design before implementation. The definition of the probability of failure is based on histogram fitting with a probability density function. The literature recommends a reliability analysis for sigma levels greater than two [27]. The frequently used reliability analysis methods are the First-order reliability method, global approximation with support points from robustness samples, and Adaptive Response Surface Method (ARSM). The method used will vary depending on the nature of the problem solved. [27].

The proposed optimization method is summarized, as shown in Fig. 3, so it can be easily adapted to any wireless power transfer optimization problem. Initially, the IPT system design specifications are identified, and the optimization problem is formulated where the design variables, objectives, and constraints are determined for the selected coil structure. The constraints are determined based on specifications of the power electronics system, compensation requirements, industry standards, and the characteristics of the coil structures. The sensitivity analysis identifies the impact of design variables on the objectives and constraints of the coil design. The number of design variables considered for the optimization process can be reduced depending on the outcome of the sensitivity analysis. The RMOO optimization performed using an optimization algorithm determines the Pareto-optimal solutions, and the safety level is calculated using robust evaluation. If a design violates the robust criteria, the constraints are modified to meet the target safety levels, and the optimization is repeated with the modified constraints. The accuracy of the final robust design is verified through reliability analysis, and if the design fails the reliability analysis, the algorithm will revert to the modification of constraints. Section IV will demonstrate the application of the proposed RMOO methodology to realize a robust coupler.

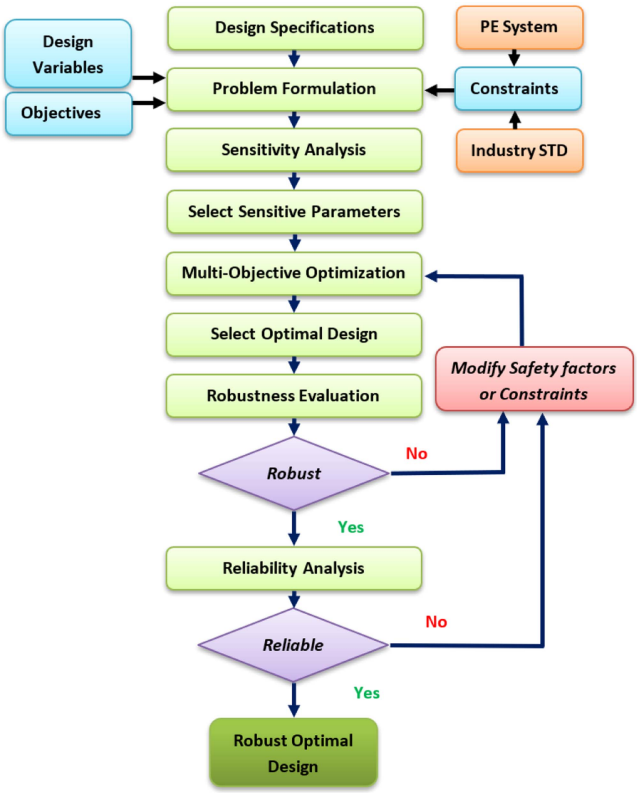

FIGURE 3. Proposed robust multi-objective optimization (RMOO) flowchart for a wireless power transfer coupler.

IV. DESIGN EXAMPLE

This article utilizes SS-compensated IPT system with a circular coupler to demonstrate the efficacy of the proposed robust optimization methodology. However, it can be applied to other coupler structures and compensation topologies proposed in literature by identifying their relevant design variables, objectives, and constraints [1].

A. DESIGN SPECIFICATIONS OF THE WPT SYSTEM

Initially, the power electronics system parameters of the SS-compensated IPT system are identified depending on the application. The parameters related to this work are listed in Table 2. The optimization is carried out for a 3.7 kW IPT system. The maximum input and output DC voltages are restricted to 350V. The AC equivalent resistance (R_{ac}) is derived using (2). The operating frequency of the IPT system is 85 kHz, while $I_{Tx(peak)}$ and $I_{Rx(peak)}$ are the AC peak values of transmitter and receiver side currents. The impact of selecting an SS-compensation topology is discussed under constraints Section IV-B4. The coupler optimization is carried out for a 3.7 kW IPT system operating at 85 kHz.

TABLE 2. WPT System Parameters

Parameter	Value
Output power (P)	3700 W
Input dc link voltage (V_{Txdc})	<350 V
Output dc link voltage (V_{Rxdc})	≤350 V
DC load resistance (R_L)	33.11 Ω
Equivalent resistance (R_{ac})	26. 84 Ω
Operating frequency (f)	85 kHz
$I_{Tx(peak)}$ (A)	23.40 A
$I_{Rx(peak)}$ (A)	16.60 A

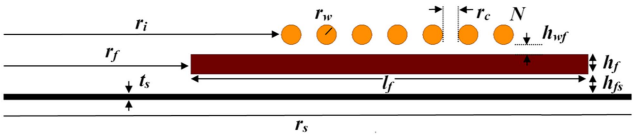

FIGURE 4. Two-dimensional side view of a circular coil structure illustrating its design variables.

TABLE 3. Ranges of Design Variables, CoV, and Design Variables of RMOO

Design Variables	Lower Bound (mm)	Upper Bound (mm)	*(CoV)%	RMOO design (mm)
r_i	75	140	1	102.24
r_w	1	2.5	20	1.907
r_c	0.5	8	25	0.59
r_s	267	320	1	298.2
h_{wf}	0.5	5	7.75	1.45
h_{fs}	0.5	5	10	2.5
t_s	0.4	2	17.5	0.75
r_f	80	98	4	80.5
N	15	20	NA	17
t_f	25		0.78	25
w_f	25		0.78	25
l_f	202		0.25	202
h	150		1	150

*(CoV)- Coefficient of Variation, RMOO- Robust Multi-objective Optimization

B. PROBLEM FORMULATION

This section identifies the design variables, objectives, and constraints to formulate the optimization problem discussed in this article.

1) DESIGN VARIABLE IDENTIFICATION

A circular coupler is characterized by the following variables, as shown by Fig. 4: radius of the conductor (r_w), starting radius of the coil (r_i), separation between two adjacent conductors (r_c), length (l_f) of ferrite (FE), thickness (h_f) of FE, width (w_f) of FE, separation between the conductor and FE (h_{wf}), separation between the FE and shield (h_{fs}), thickness(t_s) and radius(r_s) of the shield, FE starting (r_f) and number of turns (N). The design variables matrix is given by:

$$d = \left[d_1, ., d_{k_d}\right] = \left[r_w, r_i, r_c, l_f, h_f, w_f, h_{wf}, h_{fs}, t_s, r_s, r_f, N\right] \quad (28)$$

2) DESIGN VARIABLE TOLERANCES

Traditional wireless power transfer optimization problems do not consider the tolerances of design variables [3], [4], [5], [6], [7], [8], [9], [10], [11], [12], [13]. Therefore, this article introduces the coefficient of variation (COV) to quantify the tolerances of design variables. It is given by:

$$COV = \frac{\sigma}{\mu}.100\% \quad (29)$$

μ and σ are the mean and standard deviation of the design variables that have a normal distribution. The standard deviation of the design variables' manufacturing process can be estimated using the process capability index. It is given by:

$$C_{pK} = \min\left[\frac{U_{SL} - \mu}{3\sigma}, \frac{\mu - L_{SL}}{3\sigma}\right] \quad (30)$$

where U_{SL} and L_{SL} are the upper and the lower tolerance limits. C_{pK} for an existing manufacturing process is around 1.33 [18].

Therefore, the design variables tolerances are determined using (29) and (30) for a standard manufacturing process and from the manufacturer datasheets. They are listed under Table 3 in terms of the coefficient of variance, and a statistically normal distribution is assumed. Note that the number of turns does not have tolerances.

3) OBJECTIVES IDENTIFICATION

The proposed RMOO aims to maximize coil-coil to efficiency ($\eta_{cc,max}$) [19] and minimize leakage magnetic field (B_s) evaluated at 650 mm from the center of the coil, with the assumption that the Rx coil is fixed at the center of a 1.7 m wide small vehicle. Moreover, $\eta_{cc,max} > 95\%$ and $B_s < 27$ μT constraints are also considered in this design example. The considerations for achieving this will be discussed in Section IV-E and F.

4) CONSTRAINTS IDENTIFICATION

The coil design needs to consider the constraints imposed by the power electronics system and compensation topology design, STDs, and other limitations identified in the literature. The selected compensated network and its design methodology impose constraints on inductances and coupling coefficient, as identified in Section II. Equation (7) imposes a limit on the Rx-side inductance to reduce the current harmonics due to the non-linearity of the inverter and rectifier. Therefore, $L_{Rx} \geq 186$ μH according to (7). A voltage transfer ratio of $\sqrt{2}$ will result in identical coils and it also implies that $L_{Tx} \geq 186$ μH according to (10). The coupling coefficient of the design should be approximately less than 0.191, according to (8), to avoid the frequency bifurcation phenomena in the input impedance, reduce current harmonics. 150 mm air gap (h) is considered in this article. The coil area (A_C) is limited to 0.30 m^2 by considering the flux height of a circular coil is

TABLE 4. IPT System Constraints

Parameter	Value
L_{Rx}	> 186 µH
L_{Tx}	> 186 µH
k=k_s	< 0.191
h	= 150 mm
f	= 85 kHz
A_c	<30 m^2
B_{Fe}	<200 mT

TABLE 5. Coefficient of Prognosis Matrix of Design Variables, Objectives and Constraints

	Design Variables							
	r_w	r_i	r_c	h_{fs}	h_{wf}	r_s	t_s	r_f
Objectives								
η_{coil}	24	11	45	0	0	18	0	1.5
B_s	2	53	42	0	0	1	0	0
Constraints								
L_{Tx}≈L_{Rx}	10	60	29	0	0	0	0	0
k	11	18	70	0	0	0	0	0.4

1/4 of its diameter [2]. The operating frequency (f) is 85 kHz as the TIR J2954 STD limits the operating frequency to 81.38 - 90.00 kHz band to avoid interferences with other electronics of an EV. Flux density of ferrite bars (B_{Fe}) limited to 200 mT as this application falls under WPT 1 power class according to TIR J2954 STD [2]. Table 4 summarizes these constraints.

C. SENSITIVITY ANALYSIS

The coils are designed using the ANSYS Maxwell finite element analysis software, and the RMOO is performed with the tools available in the optiSLang software [28]. The lower and upper bounds of a circular coil's design variables considered for optimization are listed in Table 3.

Initially, a sensitivity analysis is performed. The influence of the design variables on the objectives and the constraints are evaluated using 100 design samples with the Advanced Latin Hypercube (ALH) sampling using the design of experiment (DOE) technique [20]. The Meta-model of optimal prognosis approach quantifies the importance or the sensitivities of the design variables [20]. The results are illustrated in Table 5 as a coefficient of prognosis matrix. Table 5 shows the impact of each design variable on objectives and constraints in terms of percentages. The design variables r_i, r_c, and r_w have the highest impact on all the objectives and the coil's constraints. The coil radius and radius of the shield (r_s) are the main parameters that impact the magnetic field measured at a point in the surrounding environment according to Biot Savart laws. In this article, coil radius is a function of r_i, r_c, and r_w. The self-inductances of planar coils are a function of r_c, r_w, r_i , as shown in [21]. A generalized analytical model to calculate the mutual inductance of two planar coils is derived from Neumann's integral of constant current-carrying filament with a Taylor expansion approach [22]. According to the derived analytical equations, the radius of the coil mainly impacts the mutual inductance. Therefore, mutual inductance is also a function r_c, r_w, r_i. The coupling coefficient (k) value depends on self and mutual inductances. However, both self and mutual inductances are a function of r_c, r_w, r_i. Therefore, k is also a function of r_c, r_w, r_i. Another analytical method to determine the coupling coefficient-based magnetic flux is given in [23]. The magnetic flux is a function of r_f. Therefore, the k is also a function of r_f. The transmission efficiency is a function of the coils' self-inductances, k, and losses, as shown in [3], [9]. The losses of the coils consist of winding losses, core losses, and shielding losses [1]. The winding losses are a function of the design variables $r_{w,}$ while shielding losses are a function of r_s as it is a variable in calculating the resistance of a shield according to [24]. The core losses depend on the volume of the ferrite, and the volume is a function of r_f. Therefore, transmission efficiency is a function of r_c, r_w, r_i, r_s and r_f. The proposed sensitivity analysis identified these relationships, as shown in Table 5.

The design variables h_{fs} , h_{wf} , and t_s have a negligible impact on the design objectives and constraints and can be neglected during optimization. The rest of the design variables have a significant impact, as shown by higher percentage contributions in Table 5. Therefore, r_c, r_w, r_i, r_s, and r_f, are considered in the optimization process, whilst the other design variables are kept constant at their initial design values. Sensitivity analysis is a relative measure of impact for the formulated optimization problem and may not be true for different optimization scenarios and coil structures.

D. DETERMINISTIC OPTIMIZATION EXAMPLE

This article uses conventional optimization to compare the proposed robust optimization methodology. Therefore, traditional optimization is initially performed, which can be found in [3], [4], [5], [6], [7], [8], [9], [10], [11], [12], [13] for wireless power transfer couplers.

The conventional DMOO will follow the following steps to determine the Pareto-front (PF) of the design [3], [4], [5], [6], [7], [8], [9], [10], [11], [12], [13] and [25].

- Minimize or minimize the functions:

$$f_{\text{ncc,max}}\left(d_1, d_2, \ldots..d_{k_d}\right) \rightarrow \max \tag{31}$$

$$f_{Bs}\left(d_1, d_2, \ldots..d_{k_d}\right) \rightarrow \min \tag{32}$$

where $f_{\text{ncc,max}}(d)$ and $f_{Bs}(d)$ are the coil-to-coil efficiency and leakage field optimization functions.

- Provided that:

$$L_{Rx}\left(d_1, d_2, \ldots, d_{k_d}\right) \leq 186\ \mu H; \tag{33}$$

$$L_{Tx}\left(d_1, d_2, \ldots, d_{k_d}\right) \leq 186\ \mu H \tag{34}$$

$$k\left(d_1, d_2, \ldots, d_{k_d}\right) < 0.191; \tag{35}$$

$$f_{\text{ncc,max}}\left(d_1, d_2, \ldots..d_{k_d}\right) > 95\% \tag{36}$$

$$f_{Bs}\left(d_1, d_2, \ldots..d_{k_d}\right) < 27\ \mu\text{T} \tag{37}$$

$$A_c\left(d_1, d_2, \ldots..d_{k_d}\right) < 0.30\ \text{m}^2 \tag{38}$$

$$B_{Fe}\left(d_1, d_2, \ldots..d_{k_d}\right) < 200\ \text{mT} \tag{39}$$

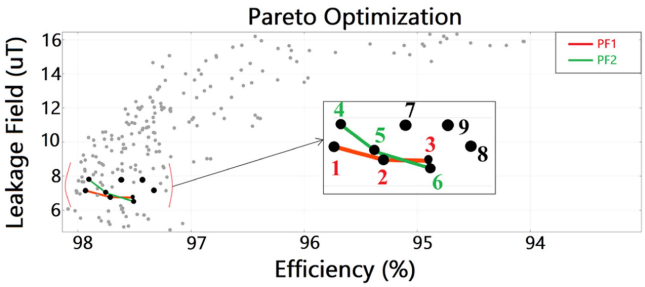

FIGURE 5. Pareto optimization results for DMOO method and RMOO method.

$L_{Rx}(d)$, $L_{Tx}(d)$, $k(d)$, $f_{\text{ncc,max}}(d)$, $f_{Bs}(d)$, $B_{Fe}(d)$ and $A_c(d)$ are the constraint inequality functions. These constraints are listed in Table 4 as well.

- For design variables

$$d_j \in [d_L, d_U] \subset \mathbb{R}^{k_d} \tag{40}$$

(40) is similar to the design variable matrix defined by (28).

$$d_L \leq d_j \leq d_U \tag{41}$$

d_L and d_U are the upper and lower search bounds of the design variables defined in Table 3. The sensitivity analysis results were used to determine the upper and lower limits. The Pareto-front is derived using the (21) for the design variables defined by (28) for a circular coupler. Fig. 5 shows the results of the Pareto-optimization of both DMOO and proposed RMOO. The design points of DMOO and proposed RMOO are superimposed in Fig. 5. These data points were generated using a non-dominated sorting genetic algorithm II (NSGA II) optimization algorithm in conjunction with ANSYS Maxwell simulations.

The Pareto-front PF1 shown in Fig. 5 corresponds to the results from the DMOO. Design points 1, 2 and 3 are on the PF1, while design points 7 and 8 are non-pareto optimal designs corresponding to DMOO. These two designs did not violate the constraints identified in Table 4. But they are not optimal. Other gray points represent the designs that violated these constraints. Note that the gray points shown in Fig. 5 are for both DMOO and RMOO results. All these gray design points are not critical as they violated the design constraints. Therefore, these designs are not suitable for implementation. The results corresponding RMOO are discussed in Section IV-F.

E. ROBUSTNESS ANALYSIS

This article introduces a safety margin to quantify the failures or violations of the target due to the uncertainties of design variables discussed in Section IV-B2. A safety level is introduced in terms of Sigma. Sigma is a statistical measure of variability in a manufacturing process. Usually, a 4.5 sigma (4.5 σ) level is acceptable for the manufacturing process, as the area of a normal distribution beyond 4.5 sigma from the mean will result in a probability of or 3.4 failures/violations per million designs due to the uncertainties of design variables

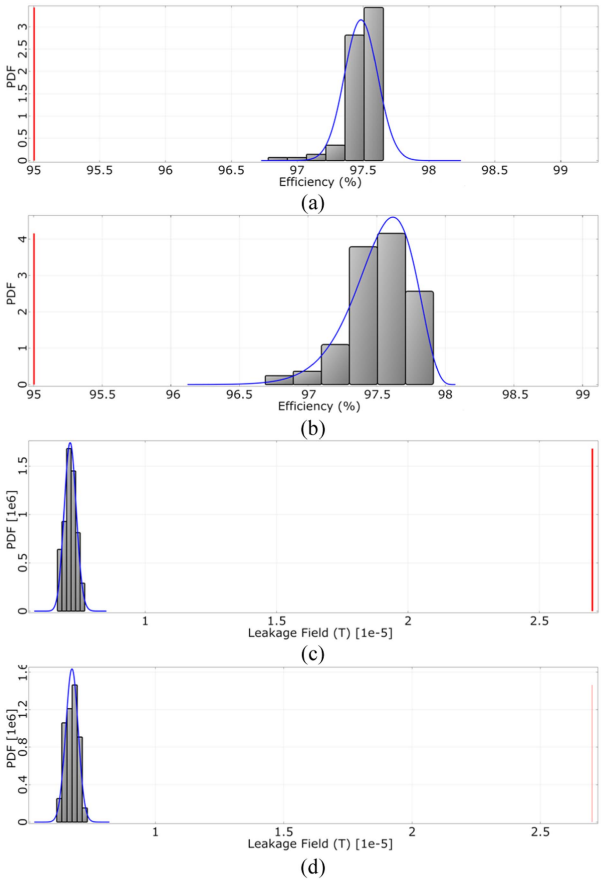

FIGURE 6. Probability density functions of designs: (a) Efficiency of DMOO design 3, (b) Efficiency of RMOO design 6, (c) Leakage magnetic field of DMOO design 3 with safety limit at 27 μT, (d) Leakage magnetic field of RMOO design 6 with safety limit at 27 μT.

[20]. Therefore, 4.5 σ is considered for efficiency, leakage flux, coupling coefficient, and Tx and Rx side inductances.

The robustness of each designs on the PF1 of the DMOO shown in Fig. 5 is evaluated using 100 design samples with ALH sampling in optiSLang [28]. The probability distribution of the objectives of design 3 is plotted with their safety margins, as shown in Fig. 6(a) for efficiency and in Fig. 6(c) for leakage magnetic field. The lower safety limit of efficiency is defined as 95%, while the upper limit of leakage magnetic field is 27 μT as defined under the SAE J2954 STD to evaluate the robustness of the design [2]. Both limits are more than 10σ safe when compared to the target safety level 4.5 σ. Therefore, the efficiency and leakage field objectives are robust.

However, as shown in Fig. 7(a), the lower bound of Rx inductance L_{Rx} is 186 μ according to design (7), which is 3.36 sigma safe. The target limit is 4.5 σ for L_{Rx} as well. This means the design does not meet the target for L_{Rx}.

The upper bound for coupling coefficient(k) is 0.191, according to (8), which is 0.90σ safe as shown in Fig. 7(c). Yet again coupling coefficient also does not meet the target safety level of 4.5 σ. This violation is visible in Fig. 7(c) due to tolerances, as several designs are above 0.191. Therefore, the optimized design 3 from DMOO is not robust in terms

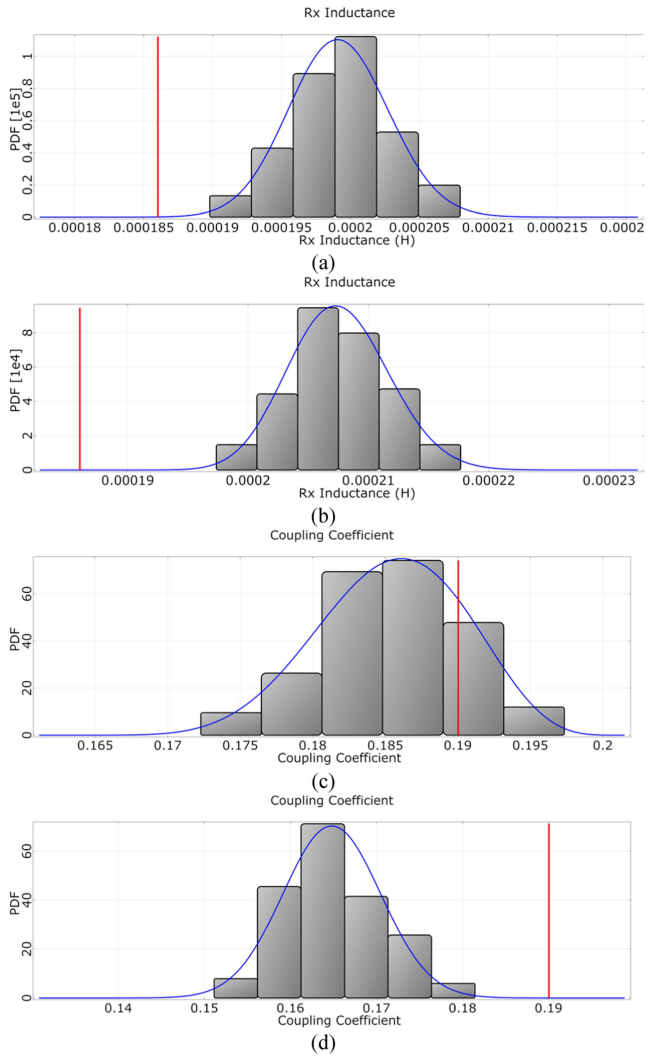

FIGURE 7. Probability density functions: (a) L_{Rx} of DMOO design 3, (b) L_{Rx} of RMOO design 6, (c) k of DMOO design 3, (d) k of RMOO design 6.

of the constraints L_{Rx} and k. Therefore, the implemented IPT system may violate inequalities (5)–(8) and (10) due to uncertainties of design variables. This is often the shortcoming of deterministic optimization. Table 6 summarizes the results of the other two Pareto optimal designs (1 and 2) from DMOO in meeting the 4.5 sigma robustness level. The results are demonstrated for the efficiency, leakage magnetic field, L_{Rx}, and k within brackets, while Yes (Y) and No (N) demonstrate whether the design meets the robust criteria. Designs 1 and 2 also do not meet the robust criteria. Detailed evaluations of these designs are not provided in the interest of space.

F. PROPOSED ROBUST OPTIMIZATION EXAMPLE

As discussed in Section III-E, DMOO given by (31)–(41) did not incorporate stochastic restrictions (SR). Therefore, SRs are introduced in robust optimization according to (22) to ensure the predefined probabilities of failure are not violated and target variances are met. In this work, the target

TABLE 6. Evaluation of Robustness Criteria of Designs From DMOO and RMOO

	DMOO			RMOO		
DN	1	2	3	4	5	6
η (%)	Y (97.92)	Y (97.71)	Y (97.55)	Y (97.90)	Y (97.75)	Y (97.50)
B_L (μT)	Y (7.14)	Y (6.74)	Y (7.50)	Y (7.80)	Y (7.06)	Y (7.40)
L_{Rx} (μH)	N (202.5)	N (201.6)	N (199.2)	Y (210.1)	Y (208.8)	Y (207.6)
k	N (0.188)	N (0.187)	N (0.185)	Y (0.168)	Y (0.166)	Y (0.164)

DN- Design Number shown in **Fig. 5**, η - Efficiency, B_L - Leakage magnetic Field, L_{Rx}- Receiver side inductance, k – Coupling coefficient, Y- Yes and N – No

probability $P^T(\mathcal{F})$ defined in (22) is 3.40 $x10^{-6}$ or 3.4 failures/violations per million designs due to the uncertainties of design variables. Equation (22) ensures that designs will not exceed the predefined $P^T(\mathcal{F})$, under the consideration of random influences defined by (24). These random influences are the tolerances of design variables determined using (29) and (30) and shown in Table 3 in terms of COV.

These considerations ensure that the objectives and constraints satisfy the predefined probabilities defined in (22) under the random influences of design variables. The objectives and constraints defined by (31)–(39) become nondeterministic functions due to random influences. Therefore, the objectives and constraints are improved with the requirement to minimize the variances $\sigma^2_{X_i}$ defined by (27). The objectives become:

$$f_{\text{ncc,max}}\left(d_1, d_2, ..d_{k_d}, \sigma^2_{X_1}, \sigma^2_{X_2}, \ldots, \sigma^2_{X_{k_r}}, P(\mathcal{F})\right) \rightarrow \max \tag{42}$$

$$f_{Bs}\left(d_1, d_2, \ldots..d_{k_d}, \sigma^2_{X_1}, \sigma^2_{X_2}, \ldots, \sigma^2_{X_{k_r}}, P(\mathcal{F})\right) \rightarrow \min \tag{43}$$

The constraints become:

$$L_{Rx}\left(d_1, d_2, \ldots..d_{k_d}, \sigma^2_{X_1}, \sigma^2_{X_2}, \ldots, \sigma^2_{X_{k_r}}, P(\mathcal{F})\right) \leq 186\ \mu H \tag{44}$$

$$L_{Tx}\left(d_1, d_2, \ldots..d_{k_d}, \sigma^2_{X_1}, \sigma^2_{X_2}, \ldots, \sigma^2_{X_{k_r}}, P(\mathcal{F})\right) \leq 186\ \mu H \tag{45}$$

$$k\left(d_1, d_2, \ldots..d_{k_d}, \sigma^2_{X_1}, \sigma^2_{X_2}, \ldots, \sigma^2_{X_{k_r}}, P(\mathcal{F})\right) < 0.191 \tag{46}$$

$$f_{\eta\text{cc,max}}\left(d_1, d_2, ..d_{k_d}, \sigma^2_{X_1}, \sigma^2_{X_2}, \ldots, \sigma^2_{X_{k_r}}, P(\mathcal{F})\right) > 95\% \tag{47}$$

$$f_{Bs}\left(d_1, d_2, \ldots..d_{k_d}, \sigma^2_{X_1}, \sigma^2_{X_2}, \ldots, \sigma^2_{X_{k_r}}, P(\mathcal{F})\right) < 27\ \mu\text{T} \tag{48}$$

$$A_c\left(d_1, d_2, ..d_{k_d}, \sigma^2_{X_1}, \sigma^2_{X_2}, \ldots, \sigma^2_{X_{k_r}}, P(\mathcal{F})\right) < 0.30\ \text{m}^2 \tag{49}$$

$$B_{Fe}\left(d_1, d_2, ..d_{k_d}, \sigma^2_{X_1}, \sigma^2_{X_2}, \ldots, \sigma^2_{X_{k_r}}, P(\mathcal{F})\right) < 200 \text{ mT} \tag{50}$$

The Pareto-optimization is performed using NSGA II algorithm in conjunction with ANSYS Maxwell. The ***PF2*** shown in Fig. 5 is the PF corresponding to pareto-optimal designs resulting from robust optimization process. Design points 4, 5, and 6 are on the PF2, which are Pareto-optimal. Design point 9 is a non-pareto optimal design corresponding to RMOO. This design did not violate the constraints identified in Table 4. However, it is not Pareto-optimal. Other gray points represent the designs that violated these constraints, as discussed in DMOO. Note that the results of DMOO and RMOO are superimposed in Fig. 5 for a better visual comparison.

The robust analysis discussed in Section III-E is performed for design 6 shown on the PF2 of the proposed RMOO, as shown in Fig. 5. The efficiency and leakage field are more than 10σ safe, as shown in Fig. 6(b) and (d). More importantly, the safety margins corresponding to L_{Rx} and k are 5.11 σ and 5.01 σ, as shown in Fig. 7(b) and (d), which is greater than targeted 4.5 σ safety margin. Therefore, this design meets the robust design criteria. Table 6 summarizes the results of the other two Pareto optimal designs (4 and 5) from proposed RMOO in meeting the 4.5 sigma robustness level. The results are demonstrated for the efficiency, leakage magnetic field, L_{Rx}, and k within brackets, while Yes (Y) and No (N) demonstrate whether the design meets the robust criteria. Therefore, designs 4 and 5 also meet the robust criteria. Detailed evaluations of these designs are not provided in the interest of space.

G. RELIABILITY ANALYSIS OF THE OPTIMIZED DESIGN

When comparing the reliability analysis methods listed in Section III-E, ARSM uses fewer solver evaluations, and extrapolation is not used in the approximation [27]. Therefore, the probability of failure is estimated accurately by using ARSM. The calculated failure of probabilities for constraints considered in design 6 is as such: L_{Rx} ($P(\mathcal{F})=1.21*10^{-7} < P^T(\mathcal{F})=3.4*10^{-6}$) and k ($P(\mathcal{F})=1.11*10^{-7} < P^T(\mathcal{F})=3.4*10^{-6}$). Both probabilities of failures are below the target $P^T(\mathcal{F}) = 3.4*10^{-6}$. These calculations indicate that the RMOO design has fulfilled the target probability of failure and is suitable for mass-scale production.

V. EXPERIMENTAL VERIFICATION

This section will demonstrate the details of the experimental procedure and experimental results of both DMOO and proposed RMOO methods.

A. EXPERIMENTAL SETUP DETAILS

The system parameters of the IPT system are listed in Table 2. The winding, core, and passive shield are fabricated using Litz wire, ferrite, and aluminium. The Litz wire is made up of 800 strands of AWG 37. Ferrite with a permeability of 2200 was used.

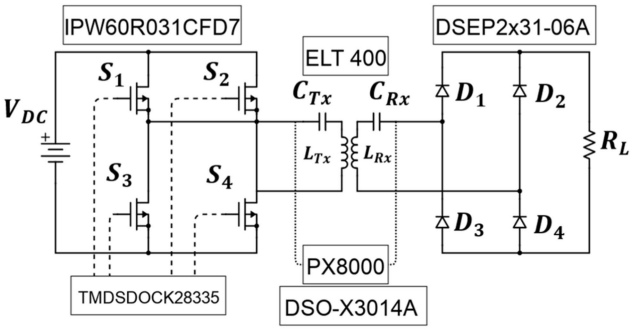

(a)

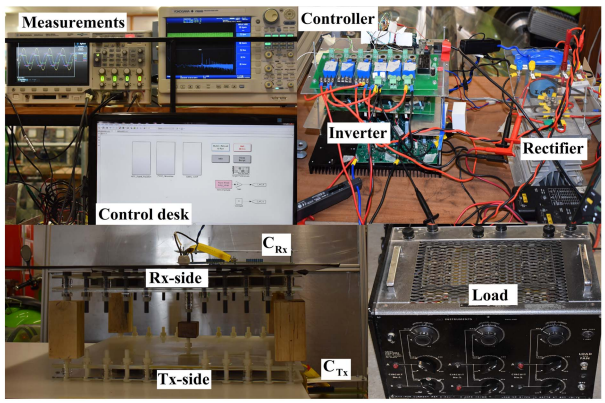

(b)

FIGURE 8. A 3.7 kW Inductive power transfer system: (a) Schematic diagram of the hardware setup, (b) Hardware prototype.

Fig. 8 shows the hardware setup used in this study. Fig. 8(a) shows the schematic diagram of the hardware setup with semiconductor devices, measuring devices, and controllers used, while Fig. 8(b) shows the actual hardware setup of the IPT system. The inverter is made up of four Infineon IPW60R031CFD7 high-voltage power MOSFETs. Texas Instrument's TMS320F28335 digital signal processor was used to implement the control related to inverter operation. The rectifier comprises two modules of IXYS DSEP2x31-06A fast recovery diodes. Two MKPC.4B 1.5 μF snubber capacitors are connected across the DC bus of the inverter to protect the switches from high-frequency switching stresses. C_{Tx} and C_{Rx} are realized using combinations of 1nF of EPCOS Metallized polypropylene film capacitors (700 VAC). A resistor bank was used as the load (R_L) to dissipate the power. Yokogawa PX8000 precision power scope was used to measure the efficiencies of the system with Agilent N2782B AC/DC probes and Tektronix differential p5200 voltage probes. Additionally, Agilent Technologies InfiniiVision 3000 DSO-X 3014A was used to capture the voltage and current waveforms. The leakage magnetic field is measured from the edge of the coupler in the lateral direction from the Tx using the Narda ELT 400 field meter. In the interest of space, the figures corresponding to RMOO are provided. However, numerical values corresponding to both DMOO and RMOO are also provided.

TABLE 7. Responses of the Deterministic and Robust Optimization Methods

DP	Deterministic Optimization			Robust Optimization		
	Sim	Imp	Δ	Sim	Imp	Δ
L_{Tx}	199.135	186.49	-12.645	207.51	188.06	-19.45
Q_{Tx}	759.66	663.99	- 95.67	791.61	669.58	122.03
L_{Rx}	199.267	185.90	-13.367	207.60	188.70	-18.90
Q_{Rx}	760.16	661.89	- 98.27	791.95	671.86	120.09
k	0.185	0.196	+0.011	0.164	0.1765	+0.0125
M	36.85	36.49	-0.36	34.22	33.25	-0.97
η_c	97.55%	96.40%	1.15%	97.5%	96.5%	1.00%
P_L	90.65	133.2	+42.55	92.5	129.5	+37
$\eta_{dc\text{-}dc}$	NA	94.30%	NA	NA	94.5%	NA
THD (I_{Tx})	3.12%	4.11%	+0.99	2.33%	2.45%	+0.12
THD (I_{Rx})	3.20%	5.01%	+1.81	3.00%	3.42%	+0.42

DP- Design Parameter, Δ= difference between experimental (imp) and simulation (sim) results, Units of L_{Tx}, L_{Rx} and M are in μH. Unit of P_L is W. η_c is the coil-to-coil efficiency, while $\eta_{dc\text{-}dc}$ is dc-dc efficiency.

TABLE 8. Evaluation of Constraints of DMOO and RMOO Designs

Cri	DMOO Design				RMOO Design			
	Sim	C	Fab	C	Sim	C	Fab	C
$8Q_e/\pi$	3.21	Y	*2.99*	*N*	3.35	Y	3.04	Y
$k< k_c$	0.185 <0.25	Y	0.196< 0.27	*Y*	0.164< 0.24	Y	0.1765 <0.266	Y
$L_{Rx}>186$	199.3 >186	Y	*185.9> 186*	*N*	207.6> 186	Y	188.7> 186	Y
$L_{Tx}>186$	199.1 >186	Y	*186.4> 186*	*Y*	207.51 >186	Y	188.1> 186	Y
$k<0.191$	0.185 <0.19	Y	*0.196< 0.19*	*N*	0.164< 0.19	Y	0.1765 <0.19	Y

Cri-Criterion, Sim- Simulated/Optimised design, Fab- Fabricated design, C- Does the design meet the criteria, Y-Yes, N-No.

B. CONFORMITY AND VIOLATIONS OF CONSTRAINTS

Design 3 from DMOO and design 6 from proposed RMOO were implemented. Table 7 lists the values of L_{Rx}, L_{Tx}, k, and coil quality factors of transmitter (Q_{Tx}) and receiver (Q_{Rx}) coils of both designs. The coils have high-quality factors at 85 kHz, which is critical for achieving high efficiency. The discrepancies in quality factors of simulated and implemented designs are mainly due to inductance variation and inaccuracies associated with estimating the parasitic resistances of the coils. Table 8 lists the design criteria (5)–(8), and (10) satisfied or violated by the simulated and implemented designs from DMOO and RMOO. The simulated here refers to the designs from the optimization process. The simulated designs from the DMOO and RMOO method satisfied all the criteria, as these designs were selected from the PFs shown in Fig. 5.

However, the fabricated coupler resulting from DMOO marginally violates the inequality (7) for L_{Rx}, while the inequality (8) is violated by a margin of +2.61%. It also violates the design criterion (5) due to violating the design inequality (7). The fabricated coupler from deterministic optimization conforms with the inequality (6) and (10). This observation is predicted during the design stage, as shown in Fig. 7(a) and (c). As discussed in Section IV-E, it failed to achieve the robust criteria on constraints (7) and (8). The fabricated coupler resulting from the proposed RMOO does not violate any inequality and conforms to the robust criteria, as shown in Fig. 7(b) and (d).

The major contributing factor for violating the inequality (8) in deterministic optimization is the design variable r_c, as it is challenging to achieve uniform r_c between the coil turns. As shown in Table 5, a small variation will significantly impact k as r_c is a design variable with the highest impact on k. Moreover, the design variable r_i of the robust optimization design is slightly varied within their assumed tolerance range from the optimized value given in Table 3. This was deliberately done to check the effectiveness of the proposed RMOO. A slight variation in design variable r_i will significantly impact L_{Rx}, L_{Tx}, and k as it has the highest impact on these parameters, as shown in Table 5.

C. EFFICIENCY AND LEAKAGE MAGNETIC FIELD ANALYSIS

The efficiency and leakage magnetic field performances of the IPT systems with the fabricated coupler from both DMOO and proposed RMOO are listed in Table 7. Power losses are 133.2 W for the implemented design from the conventional DMOO and 129.5 W for the proposed RMOO. Therefore, the robust coupler design has a lower loss component than the conventional design from DMOO.

The efficiency is measured using Yokogawa PX8000 precision power scope (20MHz bandwidth) with Agilent N2782B AC/DC probes (DC to 50 MHz, maximum current 30 Arms) and Tektronix differential p5200 voltage probes (50 MHz, ±1300 V). The transmit/receive part of the wireless power transfer system has a low power factor. The PX8000 supports the measurement of low-power-factor systems operating at very high frequencies. Moreover, its deskew function was used to compensate for and eliminate the differences between voltage and current introduced by the sensor and input characteristics in low-power-factor systems. The maximum coil-to-coil efficiency of 96.40% is reported for DMOO design, while 96.50% for RMOO design at the rated power. There is a 1 % variation compared to the final optimized solutions, but both are within the safety margin or 4.5σ boundary. More importantly, they satisfy the initial design criterion of efficiency above 95%. Fig. 9 shows the measured Tx and Rx-side current and voltage waveforms. v_{Tx} and v_{Rx} correspond to the transmitter and receiver side voltages, while i_{Tx} and i_{Rx} correspond to transmitter and receiver side currents. The frequency of these waveforms corresponds to the IPT system's resonance frequency.

The leakage magnetic field measured at 650 mm from the center of the coupler is 7.5 μT for the DMOO design and 7.4 μT for the RMOO design. Both designs are well within the safety margin and are less than 27 μT. Furthermore, the simulated and measured leakage magnetic fields are shown in Fig. 10 for RMOO design, and the maximum variation is 1.2 μT at any given point. In this design example, both objectives are satisfied by the designs derived from DMOO and RMOO.

In both designs, $k< k_c$, which corresponds to inequality (6) to avoid bifurcation. Therefore, both designs have a single-phase angle in input impedance, and the frequency bifurcation

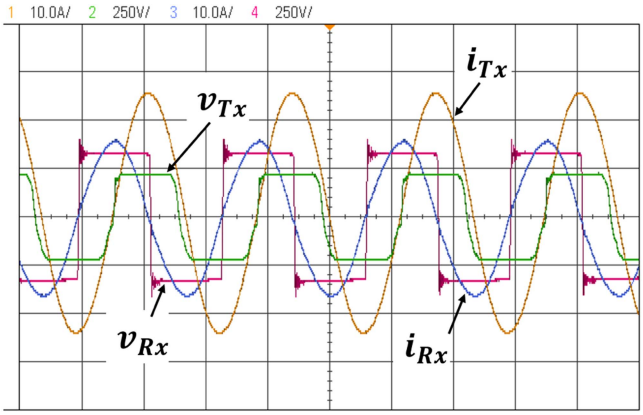

FIGURE 9. Transmitter-side and receiver-side voltage and current waveforms of the proposed robust inductive power transfer coupler (design 6).

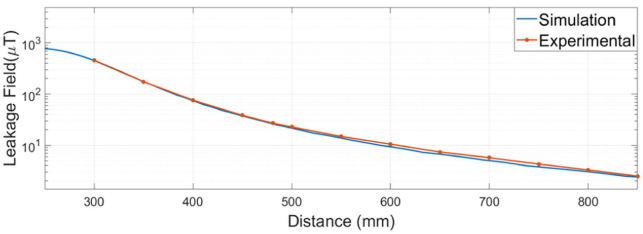

FIGURE 10. Simulated and measured leakage field from the proposed robust coupler (design 6).

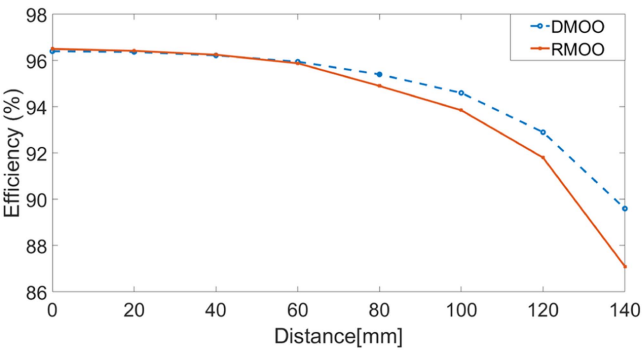

FIGURE 11. Variation of efficiency with horizontal misalignments of design 3 from DMOO and design 6 from RMOO.

is avoided. This is also evident from the high dc-dc efficiency listed in Table 7.

The efficiency of fabricated couplers from DMOO and the proposed RMOO method is also measured by displacing the receiver coil in each design along the horizontal axis at 20 mm intervals up to 140 mm. Fig. 11 shows the results of the efficiency variation with horizontal misalignments for DMOO and RMOO. Efficiency drops with an increase in misalignment for both solutions, which is expected for a wireless power transfer system due to a reduction in mutual inductance or coupling. The RMOO design has superior performance, up to 60 mm horizontal misalignment compared to DMOO. However, the efficiency is around 93.85% for RMOO, while

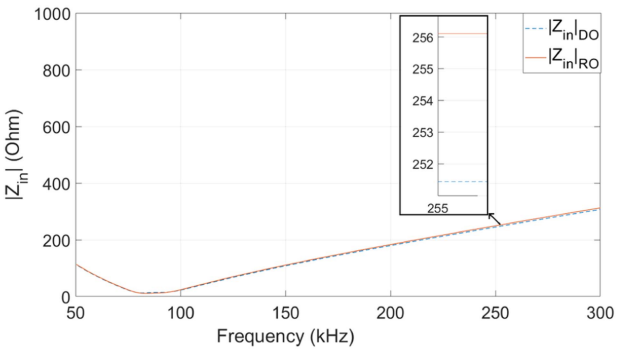

FIGURE 12. Magnitude of input impedance(|Zin|) of the design 3 from DMOO(DO) and design 6 from RMOO(RO).

94.6% for DMOO at 100 mm. The 100 mm is critical, as it is the maximum admissible horizontal offset defined in the SAE J2954 standard for EV [2].

D. TOTAL HARMONICS DISTORTION ANALYSIS

The THD of the I_{Tx} and I_{Rx} currents of DMOO and RMOO designs are evaluated to understand the impact of constraints defined by (5), (6), (7), and (8). Table 7 lists the THDs of both designs. The THD(I_{Rx}) of the fabricated design from DMOO is 1.81% higher than the optimized design. This is due to the fabricated coupler's marginal violation of constraint (5). A 0.42% increase in the THD is observed for RMOO even though it is not violating (5). However, when comparing the THD(I_{Rx}) of the implemented system from RMOO and DMOO. The THD(I_{Rx}) of RMOO is 1.59% lower than the DMOO.

The THD(I_{Tx}) of the fabricated design from DMOO is 0.99% higher than the optimized design. This is due to the fabricated coupler's violation of constraint (6). A negligible increment is observed with the design resulting from RMOO. However, when comparing the THD(I_{Tx}) of the implemented system from RMOO and DMOO. The THD(I_{Tx}) of RMOO is 1.66% lower than the DMOO. This observation can also be validated by plotting the input impedance of the IPT system, as shown in Fig. 12. The impedance difference at the 3rd harmonic is enlarged for better visualization. The harmonics of RMOO experience a larger input impedance than DMOO, hence the lower THD.

E. LOAD DEPENDENCE ANALYSIS

As shown in Table 2, the IPT system is designed for a 3.7 kW rated power, corresponding to a rated load resistance (R_L) of 33.11 Ω. Therefore, the load resistance is varied from 2 Ω to 34 Ω to understand the impact of variation in load resistance on output power. Fig. 13 shows the results of the variation of the output power of design 6 from RMOO with load resistance. The theoretical behavior is also plotted using (14). A maximum of ±15W discrepancy is observed between the theoretical and implemented design of RMOO. A similar behavior is also observed for DMOO design. It is observed

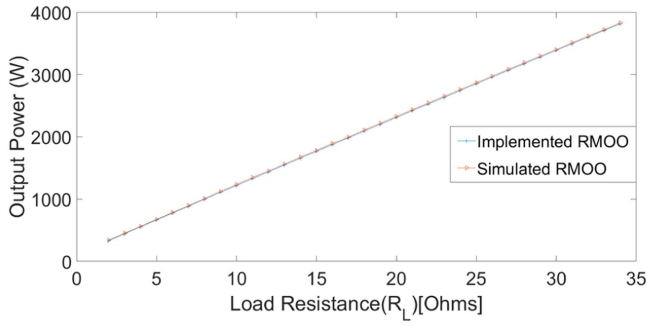

FIGURE 13. Variation of output power with load resistance of the design 6 from RMOO.

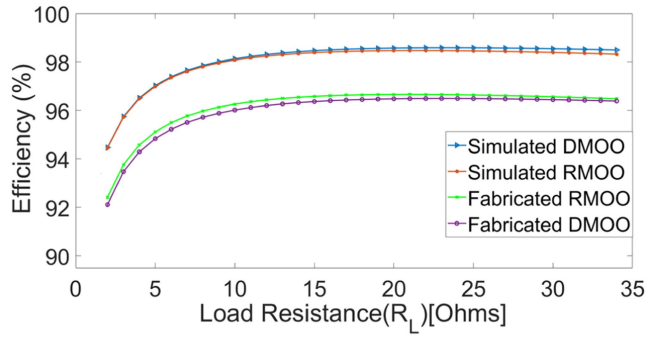

FIGURE 14. Variation of efficiency with load resistance of design 3 from DMOO and design 6 from RMOO.

that for both DMOO and RMOO, the output power increases with load resistance as output power is a function of load resistance, according to (14).

The load resistance is also varied from 2 Ω to 34 Ω to understand the impact of variation in load resistance on efficiency. Fig. 14 shows the results of the variation of efficiency with load resistance. The theoretical behavior is also plotted using (15) for the simulated parameters. It is observed that for both DMOO and RMOO, the efficiency increases at higher load conditions. The efficiency peaks around 21 Ω for RMOO and 23 Ω for DMOO. The efficiency difference is minimal between the efficiency at peak load resistance (33.11 Ω) and the resistances (21 Ω and 23 Ω) where efficiency peaks. However, the implemented RMOO has a superior efficiency profile compared to the implemented DMOO.

It is evident from the experimental results that the design from DMOO had higher total harmonics distortions due to violations of constraints related to the total harmonics distortions. However, the RMOO methodology ensured that these constraints were not violated, even at the expense of these tolerances. Hence, lower total harmonics distortions. Moreover, design 6 from RMOO has a superior efficiency profile with load variations than design 3 from DMOO. Therefore, the proposed robust optimization is beneficial in the mass-scale production of couplers, where one can incorporate these tolerances into the design process to realize a robust system. Additionally, the proposed methodology can be extended to incorporate tolerances of the compensation capacitors, resonant frequency, driving frequency, and other related tolerances of the power electronics components.

VI. CONCLUSION

The impact of uncertainties of design variables is presented in this article. The fabricated designs resulting from deterministic and robust optimization meet the efficiency and leakage field design objectives. However, the fabricated design from deterministic optimization violates THD criteria considered during optimization. This increased the THD of receiver current by 1.59% and transmitter current by 1.66% compared to robust optimization. The performance deviations are because of not incorporating uncertainties of design variables. The proposed robust optimization method demonstrated that the fabricated coupler met all the design objectives and constraints as expected. Therefore, mass-scale production of couplers in a commercial environment will benefit from the proposed methodology as the proposed design methodology incorporates the uncertainties of design variables and will produce consistently performing IPT systems. It also improves the reliability of the overall system.

ACKNOWLEDGMENT

The authors acknowledge Naomi Harrisankar, Nikhil Bejrajh, Maysam Soltanian, Riyaad Jacobs, and Hoosain Salie for their assistance in conducting this research.

REFERENCES

[1] S. Jayalath and A. Khan, "Design, challenges, and trends of inductive power transfer couplers for electric vehicles: A review," *IEEE J. Emerg. Sel. Topics Power Electron.*, vol. 9, no. 5, pp. 6196–6218, Oct. 2021.

[2] *Wireless Charging of Electric and Plug-In Hybrid Vehicles, Society of Automotive Engineers*, SAE Standard J2954, 2019. Accessed: Sep. 20, 2019. [Online]. Available: http://standards.sae.org/wip/j2954/

[3] R. Bosshard, J. W. Kolar, J. Mühlethaler, I. Stevanovi´c, B. Wunsch, and F. Canales, "Modeling and η - α-Pareto optimization of inductive power transfer coils for electric vehicles," *IEEE J. Emerg. Sel. Topics Power Electron.*, vol. 3, no. 1, pp. 50–64, Mar. 2015.

[4] A. Hariri, A. Elsayed, and O. A. Mohammed, "An integrated characterization model and multiobjective optimization for the design of an EV charger's circular wireless power transfer pads," *IEEE Trans. Magn.*, vol. 53, no. 6, Jun. 2017, Art. no. 8001004.

[5] M. Lu and K. D. T. Ngo, "A fast method to optimize efficiency and stray magnetic field for inductive-power-transfer coils using lumped-loops model," *IEEE Trans. Power Electron.*, vol. 33, no. 4, pp. 3065–3075, Apr. 2018.

[6] A. Desmoort, Z. De Grève, and O. Deblecker, "Multiobjective optimal design of wireless power transfer devices using a Genetic Algorithm and accurate analytical formulae," in *Proc. IEEE 42nd Annu. Conf. Ind. Electron. Conf.*, 2016, pp. 4518–4522.

[7] M. Moghaddami, A. Anzalchi, A. Moghadasi, and A. Sarwat, "Pareto optimization of circular power pads for contactless electric vehicle battery charger," in *Proc. IEEE IAS Annu. Meeting*, 2016, pp. 1–6.

[8] S. Bandyopadhyay, P. Venugopal, J. Dong, and P. Bauer, "Comparison of magnetic couplers for IPT-based EV charging using multi-objective optimization," *IEEE Trans. Veh. Technol.*, vol. 68, no. 6, pp. 5416–5429, Jun. 2019.

[9] H. Kim et al., "Coil design and measurements of automotive magnetic resonant wireless charging system for high-efficiency and low magnetic field leakage," *IEEE Trans. Microw. Theory Techn.*, vol. 64, no. 2, pp. 383–400, Feb. 2016.

[10] T. Yilmaz, N. Hasan, R. Zane, and Z. Pantic, "Multi-objective optimization of circular magnetic couplers for wireless power transfer applications," *IEEE Trans. Magn.*, vol. 53, no. 8, Aug. 2017, Art. no. 8700312.
[11] Y. Liu, R. Mai, D. Liu, Y. Li, and Z. He, "Efficiency optimization for wireless dynamic charging system with overlapped DD coil arrays," *IEEE Trans. Power Electron.*, vol. 33, no. 4, pp. 2832–2846, Apr. 2018.
[12] Z. Luo, X. Wei, and G. A. Covic, "Multi-objective optimization of double D coils for wireless charging system," in *Proc. IEEE Int. Power Electron. Appl. Conf. Expo.*, 2018, pp. 1–6.
[13] A. A. S. Mohamed, S. An, and O. Mohammed, "Coil design optimization of power pad in IPT system for electric vehicle applications," *IEEE Trans. Magn.*, vol. 54, no. 4, Apr. 2018, Art. no. 9300405.
[14] V. Shevchenko, O. Husev, R. Strzelecki, B. Pakhaliuk, N. Poliakov, and N. Strzelecka, "Compensation topologies in IPT systems: Standards, requirements, classification, analysis, comparison and application," *IEEE Access*, vol. 7, pp. 120559–120580, 2019.
[15] M. K. Kazimierczuk and D. Czarkowski, *Resonant Power Converters*, vol. 9. New York, NY, USA: Wiley, 2011.
[16] C. T. Krasopoulos, M. E. Beniakar, and A. G. Kladas, "Robust optimization of high-speed PM motor design," *IEEE Trans. Magn.*, vol. 53, no. 6, Jun. 2017, Art. no. 7207304.
[17] X. Zhu, J. Huang, L. Quan, Z. Xiang, and B. Shi, "Comprehensive sensitivity analysis and multi-objective optimization research of permanent magnet flux-intensifying motors," *IEEE Trans. Ind. Electron.*, vol. 66, no. 4, pp. 2613–2627, Apr. 2019.
[18] J. M. Booker, M. Raines, and K. G. Swift, *Designing Capable and Reliable Products*. Oxford, U.K.: Butterworth-Heinemann, 2001.
[19] F. Y. Lin, G. A. Covic, and J. T. Boys, "Evaluation of magnetic pad sizes and topologies for electric vehicle charging," *IEEE Trans. Power Electron.*, vol. 30, no. 11, pp. 6391–6407, Nov. 2015.
[20] T. Most and J. Will, "Sensitivity analysis using the metamodel of optimal prognosis," in *Proc. Weimarer Optimierungs- und Stochastiktage 8.0*, 2011, pp. 1–16.
[21] B. Esteban, N. Stojakovic, M. Sid-Ahmed, and N. C. Kar, "Development of mutual inductance formula for misaligned planar circular spiral coils," in *Proc. IEEE Energy Convers. Congr. Expo.*, 2015, pp. 1306–1313.
[22] L. Qian, M. Chen, K. Cui, G. Shi, J. Wang, and Y. Xia, "Modeling of mutual inductance between two misalignment planar coils in wireless power transfer," *IEEE Microw. Wireless Compon. Lett.*, vol. 30, no. 8, pp. 814–817, Aug. 2020.
[23] K. Chen, J. Pan, Y. Yang, and K. W. E. Cheng, "Optimization of ferrites structure by using a new core-less design algorithm for electric vehicle wireless power transfer," *Energies*, vol. 14, no. 9, May 2021, Art. no. 2590.
[24] M. Mohammad, E. T. Wodajo, S. Choi, and M. E. Elbuluk, "Modeling and design of passive shield to limit EMF emission and to minimize shield loss in unipolar wireless charging system for EV," *IEEE Trans. Power Electron.*, vol. 34, no. 12, pp. 12235–12245, Dec. 2019.
[25] D. Roos, K. Cremanns, and T. Jasper, "Probability and variance-based stochastic design optimization of a radial compressor concerning fluid-structure interaction," in *Proc. Int. Conf. Comput. Methods Coupled Problems Sci. Eng.*, 2013, pp. 1475–1501.
[26] D. Roos, U. Adam, and C. Bucher, "Robust design optimization," in *Proc. Weimar Optim. Stochastic Days 3.0*, 2006, pp. 1–22.
[27] D. Roos, J. Einzinger, and V. Bayer, "Robust design optimization applied to structural, thermal and fluid analysis including manufacturing tolerances," in *Proc. Wei Optim- und Stochas. 6.0*, 2009, pp. 1–22.
[28] "optiSLang - Software for CAE-based Robust Design Optimization and FE-analysis," DYNARDO, Weimar, 2019. Accessed: Sep. 20, 2020. [Online]. Available: www.dynardo.de

SAMPATH JAYALATH (Member, IEEE) received the B.Eng. degree (Hons.) in electronic engineering from Sheffield Hallam University, Sheffield, U.K., in 2013, and the M.Sc. and Ph.D. degrees in electrical engineering from the University of Cape Town (UCT), Cape Town, South Africa, in 2016 and 2022, respectively. He is currently a Lecturer with the Department of Electrical Engineering, UCT. He also chairs IEEE IAS/IES/PELS combined South Africa chapter. His research interests include filter design, control of power converters, wireless power transfer, biomedical devices, and electromagnetic robotics.

AZEEM KHAN (Senior Member, IEEE) received the B.Sc. Eng., M.Sc., and Ph.D. degrees in electrical engineering from the University of Cape Town (UCT), Cape Town, South Africa. Previously, he was with the Electricity Utility in South Africa, Eskom, as a Maintenance Engineer and System Engineer on the turbine and generator control systems. He is currently a Professor with the Department of Electrical Engineering, UCT. His research interests include permanent magnet machine design and control of renewable energy systems.